Geoderma Regional 36 (2024) e00746

Contents lists available at ScienceDirect

Geoderma Regional

journal homepage: www.elsevier.com/locate/geodrs

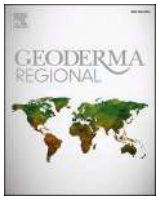

Soils surrounding saline-alkaline lakes of Nhecolândia, Pantanal, Brazil: Toposequences, mineralogy and chemistry

André Renan Costa-Silva [a,*], Yves Lucas [b], Ary Tavares Rezende-Filho [c], Mariana Dias Ramos [d], Patricia Merdy [b], Débora Ayumi Ishida [e], Laurent Barbiero [f], Adolpho José Melfi [e], Célia Regina Montes [a,e]

[a] CENA, LEST, Universidade de São Paulo, Piracicaba 13400-970, Brazil
[b] Université de Toulon, Aix Marseille Univ, CNRS, IM2NP, 83041 CEDEX 9 Toulon, France
[c] FAENG, Universidade Federal do Mato Grosso do Sul, Campo Grande 79079-000, Brazil
[d] IGCE, Universidade Estadual Paulista, Rio Claro 13506-900, Brazil
[e] IEE, LEST, Universidade de São Paulo, São Paulo 05508-010, Brazil
[f] GET, IRD, CNRS, UPS, OMP, Toulouse 31400, France

ARTICLE INFO

Keywords:
Pantanal
Nhecolândia
Arenosols
Solonetz
Silcrete
Petroduric horizon

ABSTRACT

The Nhecolândia subregion of the Brazilian Pantanal, subject to a highly seasonal climate, hosts a diverse range of freshwater and saline-alkaline lakes. The latter can be green due to cyanobacterial bloom, black due to dissolved organic matter, or crystalline. Over the past two decades, numerous studies in the region have explored the connections between the lake type, the surrounding soils, and water table dynamics. However, these insights emerged from independent studies conducted at multiple sites, making their synthesis challenging and leaving questions about the differences between lake types. Our research focuses on a representative Nhecolândia site, aiming to comprehensively understand soil and lake genesis and dynamics. For each lake type, we conducted detailed toposequence soil studies, assessing particle size distribution, chemistry and mineralogy of the <2 mm fraction of identified horizons. A 49-month temporal study utilizing PlanetScope satellite data examined lake connections to the hydrographic network affected by seasonal flooding. Our findings confirmed the general organization and mineralogy of soils around saline-alkaline lakes. Notably, we identified variations in soil toposequences corresponding to different lake type. Two types of silcrete were observed: one acidic, found at the upper slopes, and the other alkaline, located at the lower slopes. We determined that, for endorheism and lake alkalinization, the presence of a ridge around a lake is insufficient. Instead, deep impermeable horizons in the lower portion of the toposequences are essential. Additionally, crystalline lakes differentiate from black and green ones due to less efficient hydraulic isolation. Our comprehensive dataset from a single site provides a valuable resource for guiding and developing more specific studies on these alkaline systems.

1. Introduction

The Pantanal subregion of Nhecolândia is part of a large lacustrine system that has developed on sandy sediments deposited from the Pleistocene to the Upper Holocene. The lakes result from the partial obstruction of river beds by small forested ridges, referred to locally as *cordilheiras*, situated in the distal section of distributary lobes stemming from the Taquari river sedimentary megafan (Assine et al., 2015). This landscape comprises over 10,000 lakes, predominantly shallow, with sizes ranging from 0.025 to 0.15 km^2 (Costa et al., 2015; Pereira et al., 2020). The lacustrine system is primarily characterized by freshwater lakes, known locally as *baías*, with around 7% being saline-alkaline lakes or *salinas*, surrounded by alkaline soils (Almeida et al., 2007; Furian et al., 2013). These saline-alkaline lakes can further be categorized

Abbreviations: DOC, Dissolved organic carbon; DOM, Dissolved organic matter; EC_S, Soil apparent electrical conductivity; EC_W, Water electrical conductivity; EG, Ethylene glycol; ODFE, Oven-dried fine earth; OMF, Organic matter free..

* Corresponding author at: Centro de Energia Nuclear na Agricultura (CENA), Universidade de São Paulo, Av. Centenário, 303, São Dimas, 13416-000 Piracicaba, São Paulo, Brasil.
E-mail address: andrerenan00@usp.br (A.R. Costa-Silva).

https://doi.org/10.1016/j.geodrs.2023.e00746
Received 2 April 2023; Received in revised form 13 November 2023; Accepted 17 December 2023
Available online 28 December 2023

based on the colour of their waters, which can vary, presenting as green due to the proliferation of cyanobacteria, black due to high concentrations of dissolved organic matter (DOM), or crystalline (Barbiero et al., 2008; Curti-Martins, 2012; Cotta et al., 2022; Pellegrinetti et al., 2022).

The Pantanal is a low-lying region with a semi-humid tropical climate characterized by dry winter and rainy summer, mainly controlled by the South American monsoon (Zhou and Lau, 1998; Sakamoto et al., 2004; Furquim et al., 2008; Furian et al., 2013). The annual precipitation and potential evapotranspiration in the region, averaging 1100 and 1400 mm, respectively, result in a negative water balance (Alho, 2008). The interaction between the regional rainfall, the stock and the discharge of groundwater, and the inflow of water from the upstream impluvium during floods generates an annual evapotranspiration rate higher than that of precipitation (Hamilton et al., 1998; Alho, 2008; Guerreiro, 2016). However, during rainy seasons, precipitation exceeds potential evapotranspiration by about 200 mm. This surplus rainfall is sufficient to leach soluble species that accumulate in the soil due to evaporation in the dry season (Hamilton et al., 1998; INMET, 2020). Consequently, the current rainfall regime alone cannot account for the presence of alkaline soils, suggesting that other contributing processes require consideration.

Numerous studies carried out in the region over the past twenty years have ruled out the hypothesis that salinity is inherited from drier periods in the past. These investigations suggest that the saline-alkaline lakes are likely isolated from the surface drainage network, forming an endorheic-type system (Fig. 1). During the rainy season, these lakes are not subject to flooding by surface water but rather recharged by rainfall or lateral groundwater flow. During the dry season, evaporation from the surface of the lake and by capillary rise from the surrounding soils concentrates the soluble species (Barbiero et al., 2002, 2008; Almeida et al., 2007; Furian et al., 2013). Some authors propose that lateral flow of fresh groundwater between the lakes may persist even in the dry season. The soils surrounding these lakes undergo alkalinization, resulting in elevated values of soil electrical conductivity (ECs), pH and dissolved organic carbon (DOC) in soil water, reaching levels of 80 $dS.m^{-1}$, 11 and 750 $mgC.L^{-1}$, respectively (Mariot et al., 2007; Barbiero et al., 2008). These soils exhibit distinctive characteristics, notably the presence of deep, low-permeability green horizons where specific secondary clay minerals like stevensite or Fe-illite are formed (Barbiero et al., 2008; Furquim et al., 2008, 2010a, 2010b; Furian et al., 2013; Andrade et al., 2020; Vidoca, 2020; Souza Oliveira et al., 2021). The three-dimensional morphology of the green horizons may govern part of the lake groundwater dynamics by creating hydrological thresholds that control the perched groundwater fluxes to or from the lakes (Sakamoto et al., 2004; Barbiero et al., 2008; Furian et al., 2013; Freitas et al., 2019). Recent geochemical modeling has demonstrated that approximately 125 years of endorheic functioning are adequate to account for the observed alkalinity levels (Merdy et al., 2022). These last authors also noted that the alkaline nature of the lakes and surrounding soils can disappear if new drainage conditions allow an export of the labile elements out of the system.

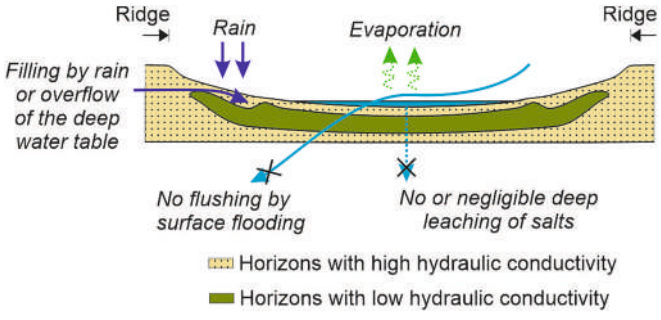

Fig. 1. Water dynamics - Main routes of water transfer in an alkaline lake according to the literature. (For colour the reader is referred to the web version of this article).

The existing body of knowledge leaves several unresolved questions. First and foremost, while it is highly likely that saline-alkaline lakes are not connected to surface drainage networks, this idea has not yet been formally confirmed through a thorough and extensive investigation. Additionally, there are uncertainties surrounding the initiation of the alkalinization process, especially the mechanisms leading to the impermeabilization of the green horizons. Lastly, there is a critical question about what exactly determines the different types of saline-alkaline lakes.

Given these unresolved questions, the goal of this study is to create a comprehensive knowledge base with three main objectives: (1) to validate the findings from previous independent studies conducted at various location in Nhecolândia, (2) to examine the influence of hydraulic discontinuities of pedological origin on the differentiation between types of lakes, and (3) to establish a foundational database for future specialized research, addressing topics omitted in this study, including the characteristics and dynamics of organic matter or detailed geochemistry.

2. Material and methods

2.1. Lake selection

Studied soils are located inside the Fazenda São Roque (19°23′26" S and 56°19′33" W), in the municipality of Aquidauana (Mato Grosso do Sul, Brazil) (Fig. 2). Four saline-alkaline lakes were selected as representatives of the southern subregion of the of Nhecolândia lacustrine system following the testing of electric conductivity (EC_W), pH, E_H and turbidity of each lake water (Table 1): one crystal-clear water lake (7-Crystalline), two black water lakes (1-Black and 6-Black) and one green water lake (4-Green) (Fig. 2). These lakes have characteristics that strongly differentiate them from freshwater lakes, whose pH and conductivity are of the order of 6.6 pH units and 143 $\mu S\ cm^{-1}$ (Costa et al., 2015). Five freshwater lakes were also considered for spatial analysis.

2.2. Spatial data

Fluviometric data, related here to the water level, were obtained through the processing of 102 PlanetScope images on Google Earth Engine platform and ArcGIS 10.5 software. This was done using the RF (Random forest) supervised classifiers within a 45-month time series, spanning from October 2017 to July 2021. This time frame was selected to address the interannual variability of precipitation. The sensor system absorbs the reflectance of targets in the visible light spectrum, as well as in the blue (455–515 nm), green (500–590 nm) and red (590–670 nm) bands, in addition to near infrared (780–860 nm), resulting in 16-bit images of radiometric information (Planet Labs, 2016). Orthorectified and atmospheric corrected (absence of clouds) 7 × 25 km images with a spatial resolution of 3 m and with a passing time between 9:30 am and 11:30 am UTC, were selected fortnightly during the defined time series. The study aimed to verify the disconnection of the studied saline-alkaline lakes from the surface drainage network. Classified areas have been defined on the image set by machine learning using the RF supervised classifier (Ramos et al., 2023), considering all available bands (NIR-R-G-B). Four classes were defined to label images: permanent water, flood channels, unvegetated soils and ridges. For each class, sample regions containing randomly distributed validation points were used to train the classifier.

A quantitative value of 1 was assigned to pixels linked with the presence of water, the value of 0.5 for pixels associated with areas subject to seasonal flooding, and a 0 value for permanently dry areas. The flood frequency map was then obtained from a reducer (*'reduce.sum'*) applied over the entire image collection. Google Earth Engine reducers allowed the acquisition of statistical and arithmetic data as they operate across the stack of images that make up the time series

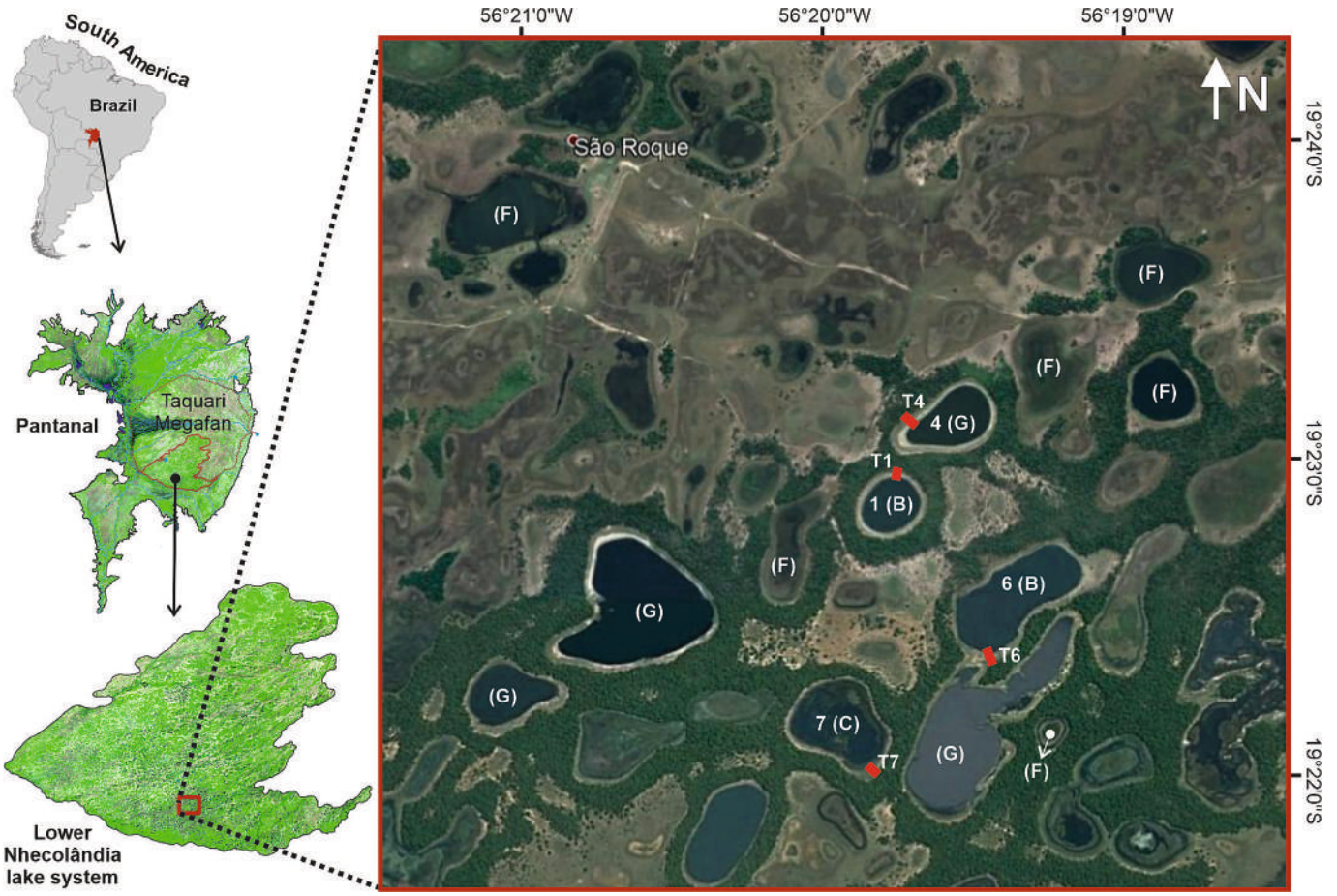

Fig. 2. Location of study - Sites in the Nhecolândia area of the Taquari megafan, Pantanal, Brazil. Saline-alkaline lakes (1, 4, 6, 7) (B: black, G: green; C: crystalline) and freshwater lakes (F). T1 to T7: toposequences associated to the studied lakes. Satellite view from Google Earth. (For colour the reader is referred to the web version of this article).

(Google, 2020).

2.3. Field work

The fieldwork was carried out at the end of the dry season, which is the time of year when motorized land access to the study site is possible, in September 2017, September 2018, October 2019 and November 2020. The soil characterization was carried out along toposequences, following the Boulet et al. (1982) method. The toposequences had a length varying from 130 to 80 m and a difference in height varying from 1.8 to 3.2 m. They were positioned on the lake slopes in regions of greater EC contrasts measured from the surface with an EM38 electromagnetic conductivity meter (Geonics Ltd., Canada), with the aim of observing the widest range of soil variations. EC measurements were carried out on bare soil in vertical dipole mode, in which the maximum investigation depth is approximately 2 m and 70% of the instrument response comes from the upper 1.5 m of the soil. Here EC measurements were not used to determined absolute values of soil parametres such as clay, water or salts content, but to realize relative values maps, making calibration relative to a given parameter unnecessary.

Microforms of local relief, lake levels and augering positions were obtained with greater that centimeter precision from topographic data collected using the Global Navigation Satellite System with Real-Time Kinematic (GNSS-RTK) positioning. Soil characteristics were collected in holes drilled with a 7 cm Ø hand auger (Eijkelkamp) and cased to prevent collapse. The auger produces reworked samples which nevertheless allow the colour, texture, nodules or concretions and subjective water content to be observed. Soil colors were obtained following Munsell Color (Firm) (1954) references. When possible, the depth, pH and EC_w of the water tables were measured at the augering time and 24 h after. Groundwater and lake water temperature, pH, EC_w and redox potential were measured in the field using a portable device (Hanna HI83140).

The nomenclature of the horizons was made according to their dominant colour and their texture, following the rules presented in Fig. 3, with notes being taken about horizons with heterogeneous colors, varied nodules, and spots associated with organic matter. Details about borehole positioning, depths, particle size distribution and pH in water for all samples are available as supplementary material.

2.4. Laboratory procedures

Soil samples were dried in a ventilated drying oven at 40 °C, crushed and sieved with a 2-mm mesh to obtain oven-dried fine earth (ODFE). When necessary, samples were ground and sieved with a 150 mesh (106 μm) and/or organic matter was removed with sodium hypochlorite (NaClO) at pH 9.5 (Anderson, 1963), resulting in powder and organic matter free (OMF) aliquots. Particle size distribution was determined by the Robinson pipette method (Pansu and Gautheyrou, 2006) and textural classes were denominated according to the USDA (1987). Clay and silt fractions were obtained by centrifugation (Jackson, 1985). It should be noted that the mode of separation of the clay fraction, which requires suspension in ultrapure water, is likely to dissolve minerals such as evaporitic minerals or very small carbonates. Soil pH was measured from the ODFE with a 1:2.5 w:w soil:water ratio (EMBRAPA, 2017). Total chemical analysis for major element determinations was

Table 1
Saline-alkaline lake data.

1-Black	*4-Green*	*6-Black*	*7-Crystalline*
Water Electrical Conductivity (EC_w - μScm^{-1})			
3500*	3420*	1662 *	826***
3340*	8730**	28240**	
8160**	2990***	1490***	
2270***	3950***	2050***	
	4990***		
	5750***		
Water temperature (°C)			
31*	27,4*	26,6*	25,5***
24,5*	26,3***	24,8***	
Water pH			
9,67*	10,30*	9,45*	8,62***
9,70*	9,76***	9,24***	
9,35***			
Water redox potencial (mV)			
+93,8*	+88,9*	+207,2*	+50,0***
+ 90,6*	+ 88,7*	+ 201,4*	
+ 88,3*	-30,0***	+ 192,1*	
-15,0***		+ 90,0***	
Sediment redox potencial (mV)			
−399,3*	−408,5*	−3,4*	−280,0***
-536,9*	-418,3*	-3,0*	
-541,3*	-430,0***	-9,7*	
-450,0***		-220,0***	
Turbidity (NTU)			
28*	>1000*	117*	1,8***
75***	466***	108***	

* Jul/17.
** Sep-Oct/17.
*** Sep-Oct/19

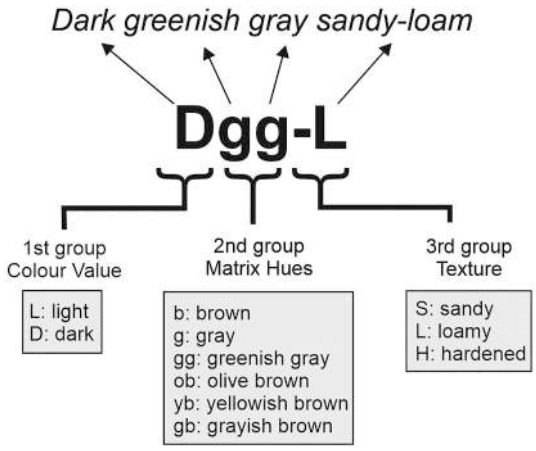

Fig. 3. Nomenclature of the horizons – Scheme of the different colour values, matrix hues and textures found in the studied soils.

performed using total melting of soil samples and measured by Inductively Coupled Plasma Optical Emission Spectroscopy (ICP-OES).

2.5. Mineralogical analysis

Most soil minerals were characterized on the <2 mm fraction by X-ray Diffractometry (XRD) and Fourier Transform Infrared spectroscopy (FTIR). Diffuse Reflectance Spectroscopy (DRS) was used for the identification of iron oxides and oxy-hydroxides. XRD samples were analyzed using a Philips PW 1877 diffractometer (Philips, Amsterdam, Netherlands) operated at 40 kV potential, 40 mA current, using CuKα radiation with a graphite crystal monochromator. The scan was performed from 3° to 90° (2θ) with a step of 0.02° and 2,5 s per time accumulation step. Mineral phases were identified on the X' Pert HighScore Plus version 4.9 software (Malvern Panalytical, Netherlands). XRD analysis was performed on the clay fraction (<2 μm) from the ODFE and OMF aliquots, oriented and saturated (1) with magnesium chloride ($MgCl_2$), later solvated with ethylene glycol (EG), and (2) with potassium chloride (KCl), later heated to 110 and 550 °C (Wilson, 1987).

Representative peaks used for mineral identification were the following: quartz, 3.34 Å, 4.25 Å and 1.81 Å; feldspars (microcline and/or orthoclase), 3.24 Å, 4.21 Å and 3.29 Å); micas (muscovite and/or illite), 4.29 Å, 3.86 Å and 10 Å; kaolinite, 7.13 Å, 3.56 Å and 4.35 Å; 2:1 expandable clay minerals (montmorillonite and/or vermiculite), 12 to 15 Å; calcite, 3.02 Å, 1.87 Å and 2.28 Å.

FTIR was performed on OMF clay mixed with potassium bromide (KBr) pellets prepared with KBr Tablet Die using a Shimadzu IR Prestige-21 spectrophotometer (Shimadzu, Japan), with spectra from 400 to 4600 cm^{-1}. Saturation or low-resolution bands were re-evaluated in replicates with lower or higher sample mass pellets. Normalization of results was achieved by the mineral phase band with the highest absorption, considering an absorbance correction factor based on mass values of sample, KBr and pellets. The identification of mineral phases was performed by characteristic absorption bands (Russell and Fraser, 1994; Ekosse, 2005; Vaculíková and Plevová, 2005; Saikia et al., 2008; Ji et al., 2009; Theodosoglou et al., 2010; Lainé et al., 2017; Acevedo et al., 2017; Zviagina et al., 2020).

The identification of iron oxides and oxy-hydroxides by DRS was performed on powder ODFE and OMF clay in a Cary 5 spectrometer (UV-VIS-NIR) (Varian, USA). The samples were analyzed in triplicate, ranging from 370 to 820 nm with increments of 0.1 nm. The reflectance R was measured in comparison to a Halon pattern and transformed into the Kubelka-Munk remission function [$f(R) = (1 - R)^2 / 2\ R$]. From the obtained curves, the second derivative was calculated and mineral phases were identified through characteristic absorption bands ^4E:^4A_i and EPT (Electronic Pair Transition) (Kosmas et al., 1984; Malengrau et al., 1996; Scheinost et al., 1998; Cornell and Schwertmann, 2000). Identification of goethite and hematite was made by comparison with characteristic absorption bands in commercial standards (Sigma-Aldrich 71,063 and 310,050, respectively).

2.6. Statistics

Principal components analysis (PCA) was performed using XLSTAT 2017 on various sets of the obtained data. PCA project multidimensional data clouds to subspace in order to minimize the residual variance, choosing the most relevant directions (principal components) in the data (Jolliffe, 2002). We chose a correlation based PCA on standardized variables to avoid sensitivity to the scaling of the variables.

Interpolated isovalue curves were established from analytical data (EC, fine fraction, pH) by ordinary kriging interpolation using the Surfer software (Golden Software, USA).

3. Results and discussion

3.1. Study site and lake characteristics

During collection of soil samples, physicochemical parameters of waters and sediments from within the selected saline-alkaline lakes (Fig. 1) were monitored and are presented in Table 1. The crystalline-type lake and the green-type lake had the lowest and highest pH and turbidity values, respectively, the black-type lakes being in between. EC_w values showed strong variations, ranging from 826 μS/cm (7-Crystalline lake on September 2019) to 28,240 μS/cm (6-Black lake on

October 2017).

The alkaline lakes showed a typical succession of vegetation from their upper part to their lower part: *cerrado* type savanna forest on the sandy ridges and a succession of savanna woodland, open woody savanna, open shrubby grassfield with palm trees and savanna grassfield on the slopes, susceptible to differentiation by the predominance of *andropogon bicorns* (*capim-de-burro*) and *cynodon dactylon* grass species (Salis et al., 2014) (Fig. 4).

The lake biota differed between lake types: it was oligotrophic vegetated for the 7-Crystalline lake, oligotrophic turbid for the 1-Black and 6-Black lakes, and eutrophic for the 4-Green lake. More details on biota can be found in a companion study to this one (Pellegrinetti et al., 2022).

3.2. Spatial analysis

The 102 PlanetScope satellite images showed that the four studied saline-alkaline lakes are all surrounded by forested sandy ridges, the altitude of which is >2 m higher than the surface of the lakes at the end of the wet season (Fig. 5). Although all taken in the same season, the views show significant variations in the levels of the lakes, resulting from the rainfall of previous months. The Fig. 6 presents the average of three meteorological stations (Nhumirim: 18°59′18"S 56°37′08"W; Coxim: 18°28′21"S 54°42′58"W; Sonora: 17°37′02"S 54°45′51"W) which accounts for the flooding in the Nhecolândia area. In October 2019 (Fig. 5B), the lakes had a rather high water level for the end of the dry season due to regular rainfall in the previous rainy season. In November 2020 (Fig. 5C), the lakes had very low water levels, with some almost dry, due to low rainfall in the previous rainy season (Fig. 6). The situation was intermediate in October 2017 (Fig. 5A). These observations underline the strong interannual heterogeneity of precipitation.

The flooding dynamics in the area are outlined in Fig. 5D. Patches of lighter blue tones within the 7-Crystalline lake are attributed to the presence of macrophytes and their spectral reflectance characteristics. The ephemeral flood channels, regionally known as *vazantes*, align with the geomorphological description provided by Cunha (1980), depicting smooth and elongated depressions that distribute the incoming floods and correspond to periodically flooded soils. The main flood channel of the area, referred to as the *Mangabal vazante*, connects with the Taquari River and play a crucial role in replenishing freshwater lakes during the rainy season (solid arrow in Fig. 5). For most freshwater lakes located outside the floodplain, it is possible to identify temporarily active connections with the floodplain (dotted arrows in Fig. 5). The saline-alkaline lakes are surrounded by forested ridges with no identifiable connection to floodplains, suggesting that they are not filled in rainy season by regional floodwaters which cannot overflow these ridges. This observation support the hypothesis that saline-alkaline lakes result from a disconnection with the superficial hydrographic network. However, some freshwater lakes also lack an identifiable connection to the floodplain network, indicating that the mere presence of a forested ridge is insufficient to ensure the disconnection that leads to the progressive alkalization of lakes.

In order to evaluate the hydraulic connection between lakes and the regional groundwater level, the water surface altitude of saline-alkaline and freshwater lakes was measured during the same day in November 2019, at the end of the dry season (Fig. 7). The freshwater lakes showed the same elevation, which could indicate the regional water table level. All alkaline lakes have different elevations of water surface, indicating a hydraulic disconnection of these lakes with regional groundwater.

3.3. Toposequences

EMC_S mapping around toposequences and borehole locations are given in Fig. 8. Several factors can result in higher EC values, such as soil moisture, clay content, and concentration of ionic species in the soil solution (Alves et al., 2013). For better visualization, the EMC_S profiles along each toposequence will be shown in toposequence figures (red lines on Figs. 9 to 12). As the EMC_S measurements were not carried out on the same day for all lakes, the values are not comparable from one lake to another.

3.3.1. T1-Black lake toposequence (Fig. 9)

The ridge soil was a homogeneous, sandy, light brown profile >2 m deep overlying a g-H indurated silcrete horizon that prevented manual augering. Such silcrete are known to form by Si liberation by silicate weathering, followed by its precipitation as secondary silica driven by supersaturation promoted by evaporation in the capillary fringe (Nash and Ullyott, 2007). The geochemical feasibility of this process in the considered soil has been confirmed by modeling (Merdy et al., 2022). Downslope, this silcrete horizon progressively turned less indurated and disappeared, with the whole profile becoming darker and greener. The deep horizons, although remaining sandy, gradually became loamier, up to 17.6% of (clay + silt) at the base of the slope. These loamier horizons had low hydraulic conductivity, as evidenced by the two different water tables observed during the surveys: a perched water table with high EC_W and pH (higher than 2.1 mS cm^{-1} and 8.2, respectively), and a deep-water table with low EC_W and pH (lower than 0.4 mS cm^{-1} and 7.1, respectively). The deep-water table was under hydraulic load: water slowly raised in the casing tube after it was reached. The low-permeability green horizons formed a marked step on the slope, favoring the hydraulic discontinuity between the ridge and the soils of the

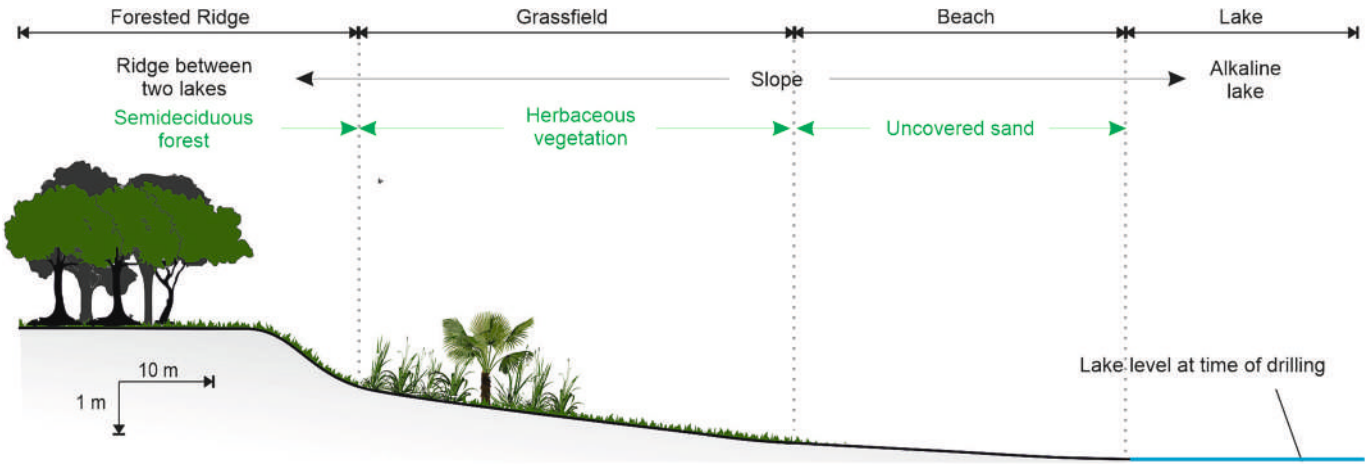

Fig. 4. Landscape units - Typical vegetation along a saline-alkaline lake slope.

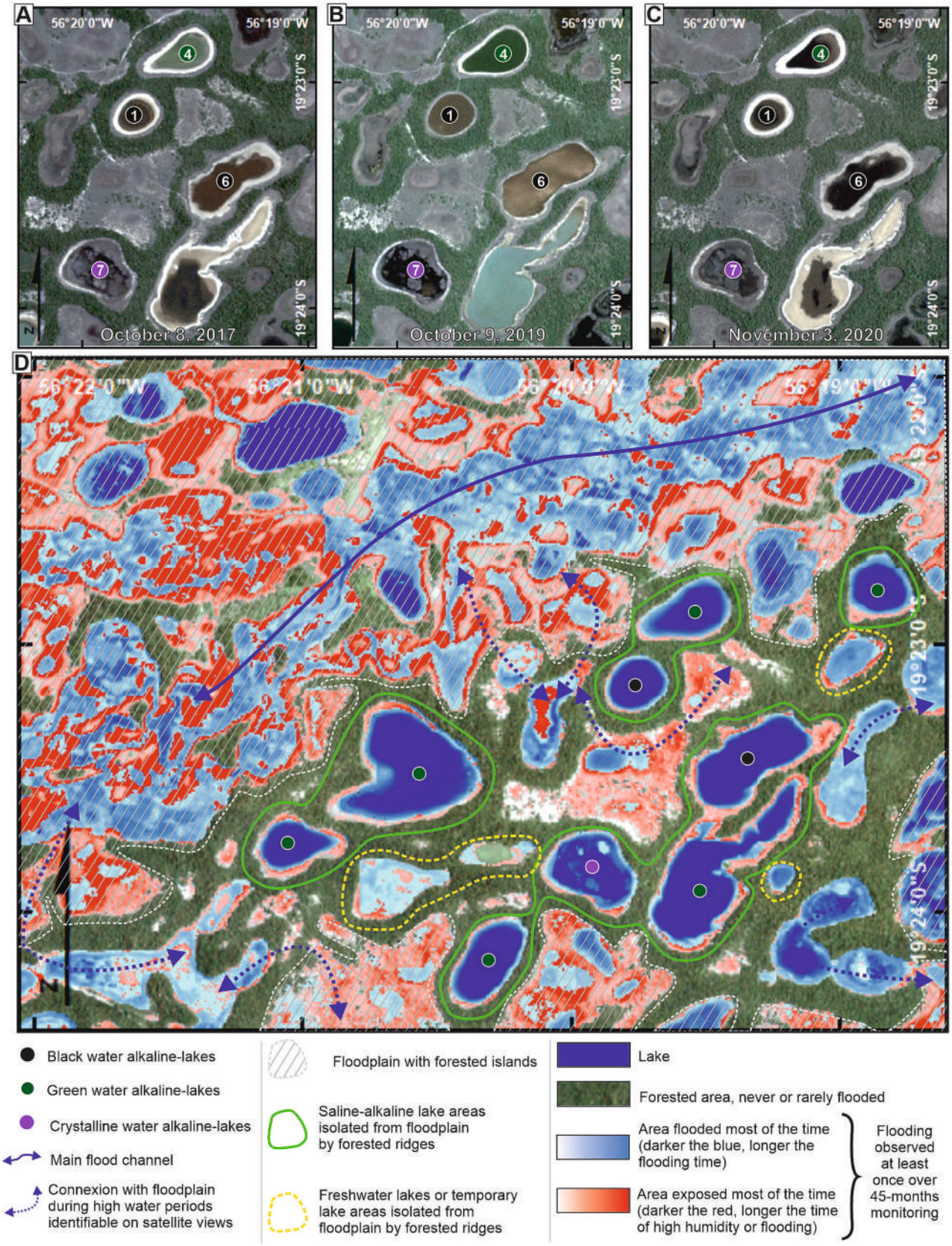

Fig. 5. Flooding monitoring - Interannual variability of the water level in the lakes studied. Satellite views from PlanetScope. (For colour the reader is referred to the web version of this article).

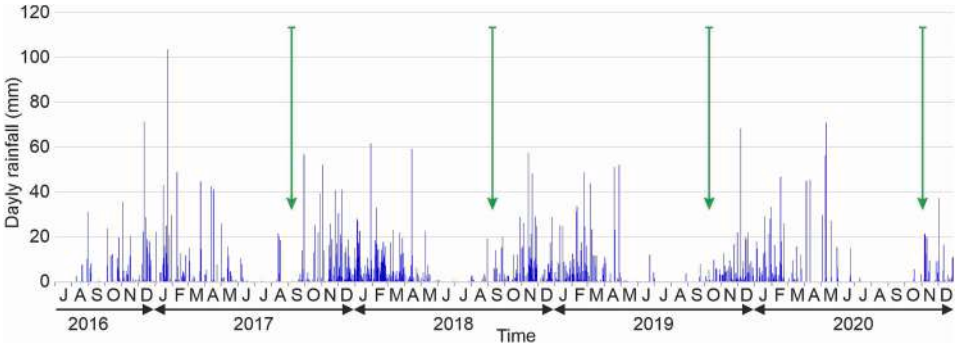

Fig. 6. Daily rainfall in the Nhecolândia area. Green arrows indicate the field work periods.

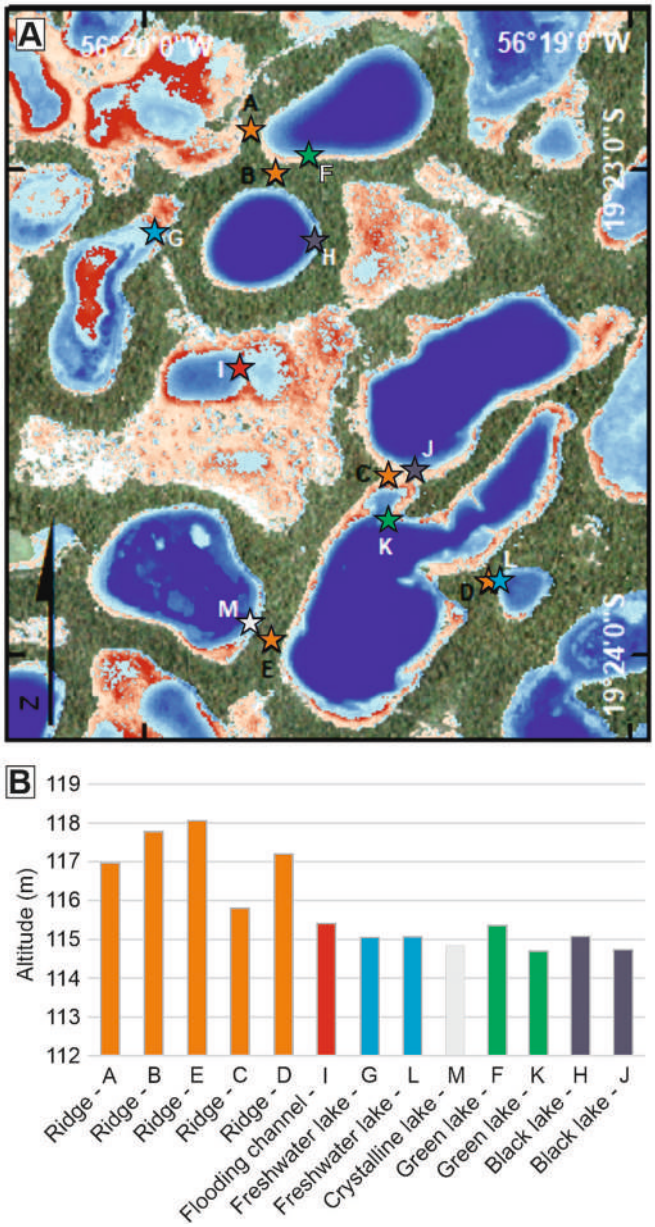

Fig. 7. Topographic data - Altitude of ridges and lake levels measured on the same day. Letters refer to points situated on the satellite view. (For colour the reader is referred to the web version of this article).

lower slope.

Soil pH (Fig. 9c) ranged from 3 to 10 within the toposequence. Ridge soil was slightly acidic, around 6–7. Topsoil horizons gradually became more alkaline downstream, reaching values >9 in the lower part of the slope, which was consistent with the gradual increase of EMC_S. Very acid horizons (hyperacidic horizons, pH < 4) were observed at depth in the lower third of the slope, resulting in a high pH contrast that went from >9 to <3 in <1 m.

Horizon geometry and characteristics, including high pH contrast, have already been observed in similar toposequences (Barbiero et al., 2008, 2016). Modeling by Merdy et al. (2022) showed that a pH between 3.2 and 3.5 can be achieved by mixing alkaline water from alkaline horizons or lakes and deep acidic groundwater, with the reduction of pH attributed to ferrolysis.

3.3.2. *T4-Green lake toposequence (Fig. 10)*

The T4 toposequence was very similar to the T1 toposequence: from the upper to the lower part of the slope, the profile progressively darkens and turns greener; (clay + silt) content increase in depth forming low hydraulic conductivity horizons isolating an alkaline perched water table from acidic deep groundwater; topsoil pH increases gradually up to 10.5; and there are hyperacidic horizons at depth in the lower third of the slope. There were, however, some differences: no indurated silcrete was observed at depth in the ridge soil; the EMC_S profile showed high values towards the middle of the slope, which could be due to a local higher accumulation of salts in topsoil horizons by capillary rise of the lake water.

3.3.3. *T6-Black lake toposequence (Fig. 11)*

Most of the similarities between T1 and T4 toposequences were observed in the T6 toposequence: horizon colour transitions, (clay + silt) content increase forming low hydraulic conductivity horizons that isolate different water tables and a gradual increase of the topsoil pH. However, some features differed. The deep groundwater was slightly less acidic (around 7.6), which could indicate less impermeable green horizons. The whole sequence had a higher (clay + silt) fraction content, which could be due to a higher fine fraction content of the parent material, as suggested by a (silt + clay) content higher than 30%, 550 cm deep, in the ridge soil. A well-developed hardened silcrete horizon was observed around 150 cm in depth from the ridge to the lower third of the slope and discontinuous topsoil silcrete horizons were also observed along the lower third of the slope. Better development of silcrete compared to the T1 toposequence could be due to higher capillary rise due to the higher content of the fine fraction or, regarding the ridge silcrete, a flow-barrier effect due to textural layering (Li et al., 2014). The EMC_S profile along the slope presented multiple peaks, which could be related to textural variations in the topsoil horizons. Acidic, not hyperacidic, horizons were observed at depth in the lower part of the toposequence, which can be due to less impermeable green horizons allowing better mixing between alkaline and acid groundwaters and

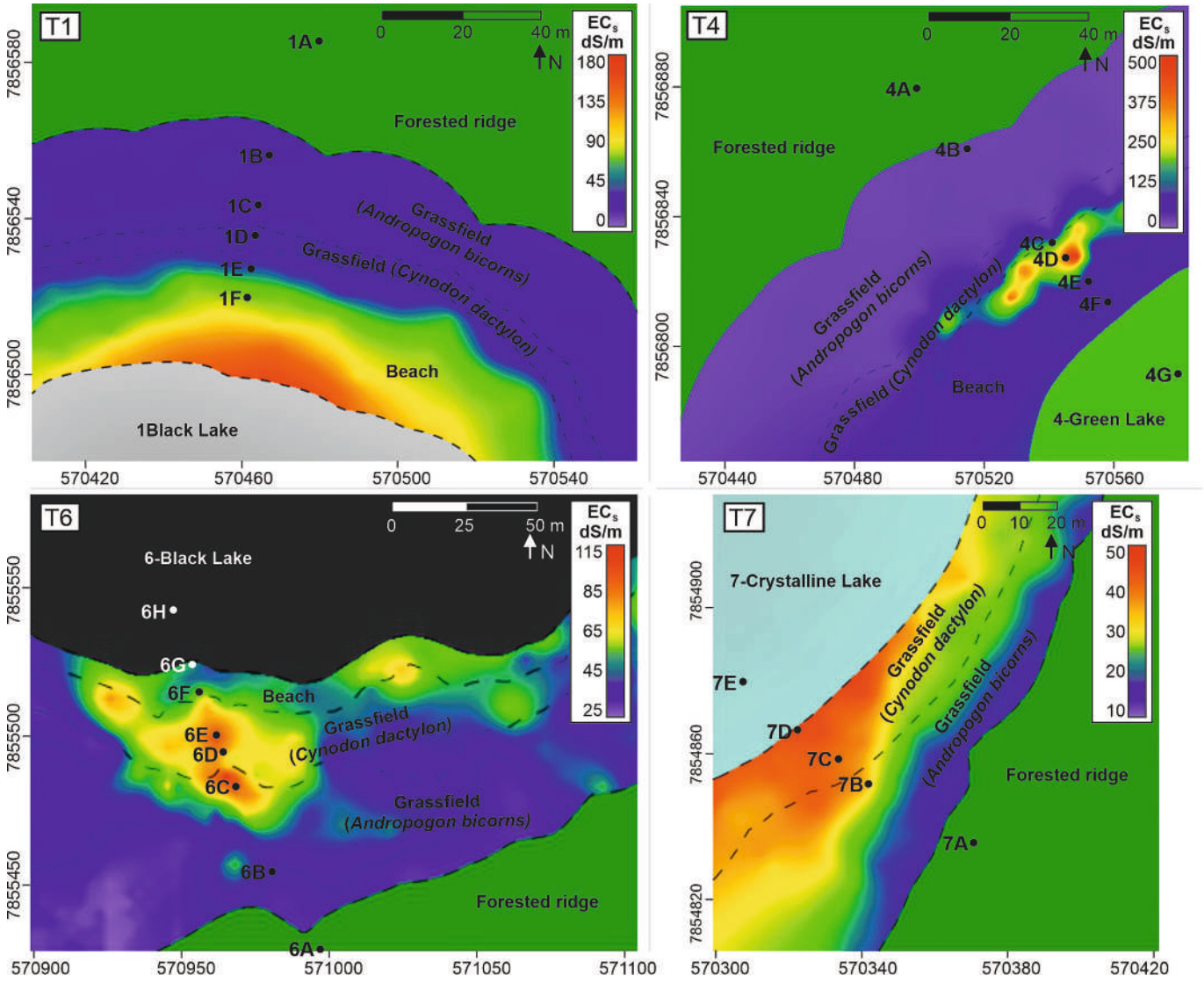

Fig. 8. Electromagnetic soil conductivity (EMC_S) mapping of soils – EMC_S values around each saline-alkaline lake selected, with the delimitation of different landscape unit areas and the positioning of all boreholes. (For colour the reader is referred to the web version of this article).

better water turnover. It is also possible that the observations were not deep enough to observe hyperacidity.

3.3.4. *T7-Crystalline lake toposequence (Fig. 12)*

The T7 toposequence ends on a less alkaline lake than the others, with the presence of shells on the beach surface and subaerial vegetation inside the lake. Like the other three toposequences, this one had soils ranging from acidic to alkaline horizons from the ridge to the lake and two distinct water tables separated by greenish horizons. The poorly permeable green horizons, however, did not form a marked step on the slope. The hydraulic discontinuity between the ridge soils and the upper soil horizons at the lower part of the slope is therefore less marked than for the other sequences. The downslope soils were slightly less alkaline than in other toposequences, with the maximum measured pH being 9.2. Consistently, the pH of the perched water table measured in 2019 had a lower EC_W value (1.1 mS cm^{-1}) than in other toposequences and was only slightly alkaline (7.2), with little difference with the deep groundwater (6.9). No hyperacidic horizons were observed at depth in the lower part of the toposequence. As for toposequence T7, the soils showed, on average, a higher fine fraction content than toposequence T1 and T4. As for the T7 toposequence, the less intense peaks in the EMCs profile along the slope could be related to horizons with less salt accumulation, in which less textural variations in the topsoil horizons causes less confinement.

3.4. *Mineralogy results*

A summary of main minerals identified by XRD, FTIR and DRS is given in Fig. 13. The main minerals identified along the toposequences were quartz, feldspars (microcline and/or orthoclase), micas (muscovite and/or illite), kaolinite, 2:1 expandable clay minerals (montmorillonite and/or vermiculite), calcite, goethite, hematite, ferrihydrite.

Quartz, feldspar and muscovite, part of illite and kaolinite are inherited from the parent sediment. These minerals were likely transported with little modification and remained restricted to the sand and silt fractions (Assine et al., 2015; Oliveira Júnior et al., 2020).

According to published studies on similar systems (Barbiero et al., 2008, 2016; Furquim et al., 2008, 2010a, 2010b; Guerreiro et al., 2019; Andrade et al., 2020), the main expected secondary minerals are Fe-kaolinite, Fe-illite, Fe-beidellite-type smectite in upslope soils, stevensite-type smectite in downslope soils, with many types of mixed-layered types from these phyllosilicate species, amorphous silica which can form silcrete nodules or horizons, and calcite. In this study we did not differentiate illite from muscovite, or types of expandable 2:1

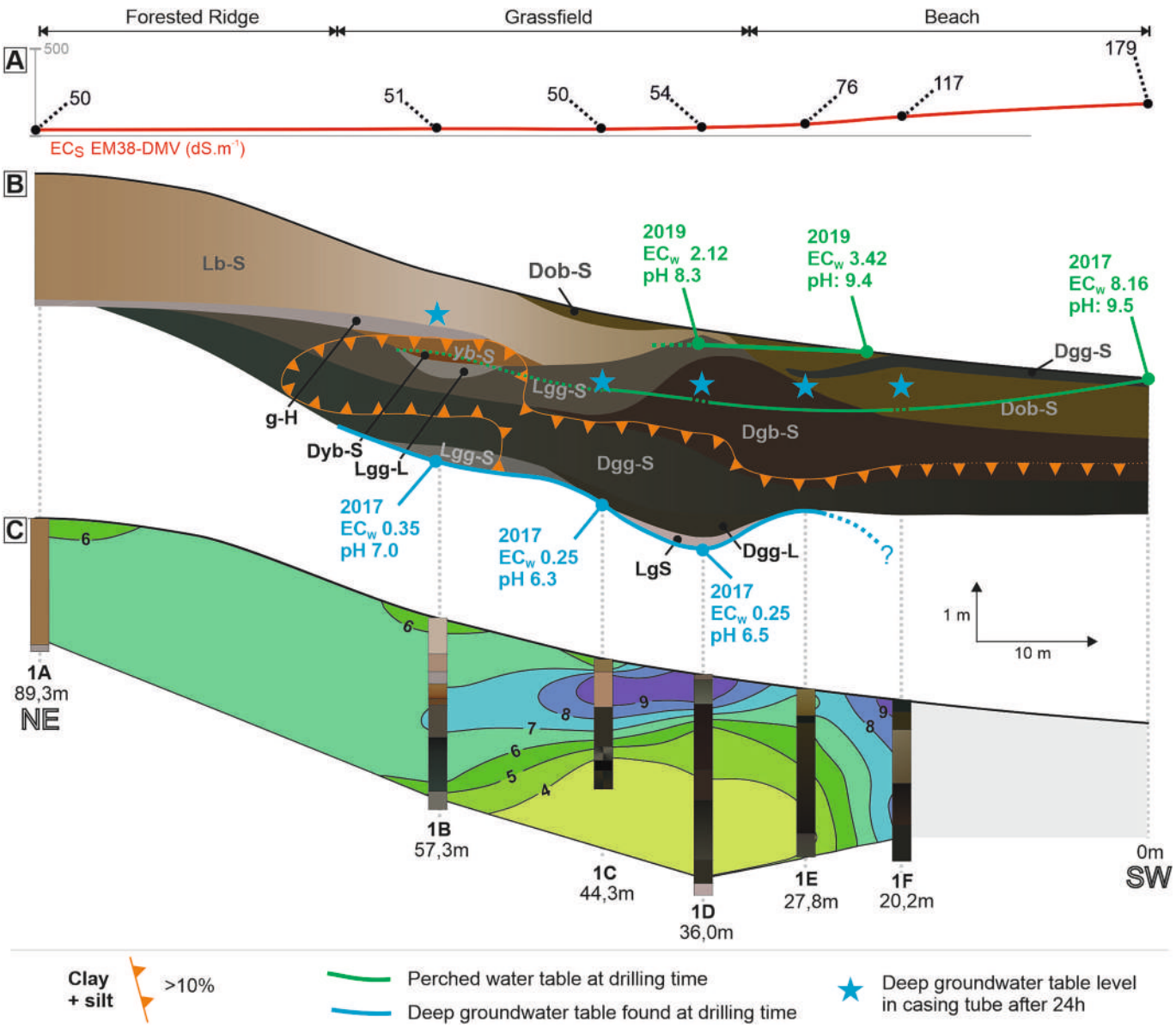

Fig. 9. T1 - Main characteristics of the 1-Black lake toposequence. (a) EMC_S profile; (b) soil horizons, water levels, fine fraction and EC_W values; c) soil pH. (For colour the reader is referred to the web version of this article).

clays. We have however noticed that expandable clays were present everywhere, except in the sandiest horizons of the upper part of the profiles. On ridges, this was expected in the leached, acidic sandy horizons where there are no conditions for the neoformation of 2:1 secondary clay minerals. On slopes, where higher pH and local carbonate precipitations attest to more confined conditions, possibly precipitated 2:1 minerals may be leached at depth or downstream by perched groundwater circulation.

Calcite was observed in high pH downslope horizons, especially in the T6 toposequence where HCl-effervescent nodules larger than 2 mm were observed. However, calcite in the other green horizons may have been overlooked due to the method of separation of the clay fraction, as described in §2.4, which has the potential to dissolve soluble minerals. These calcite nodules provide support for the hypothesis that solutes concentrate during the dry season through the evaporation of groundwater likely originating from the lake or from deeper horizons.

Amorphous silica was not identified by XRD, but its presence is most likely based on observations of hardened horizons (g-H) or non-HCl-effervescent nodules (horizons Dgg-L and Lgg-L).

These results are consistent with the results obtained by Merdy et al. (2022) using conceptual geochemical modeling on an idealized toposequence similar to those described here. While kaolinite precipitation is generally associated with wetter climates (Ishida et al., 2014), this remains possible here despite the strongly negative annual water balance. These authors, however, predict that there is precipitation of evaporitic minerals (gaylussite, pirssonite, sylvite, nahcolite, halite, glaserite) in the downslope surface horizons, none of which were observed in our study. Here too, the mode of preparation of the clay fraction is probably responsible for the non-observation of these very soluble minerals.

Regarding iron oxides and hydroxides, we did not observe in the results obtained here a correlation of their distribution with other characteristics nor a causality in this distribution. Goethite and hematite are common phases in soils, as a result of Fe-rich silicates weathering processes and may even act as a reliable proxy for local precipitation (Zhang et al., 2007). While hematite can be associated with hot and dry environments, goethite can be associated with cold and humid environments. Ferrihydrite ($Fe_2^{3+}O_3$ $0.5H_2O$) is a metastable mineral that

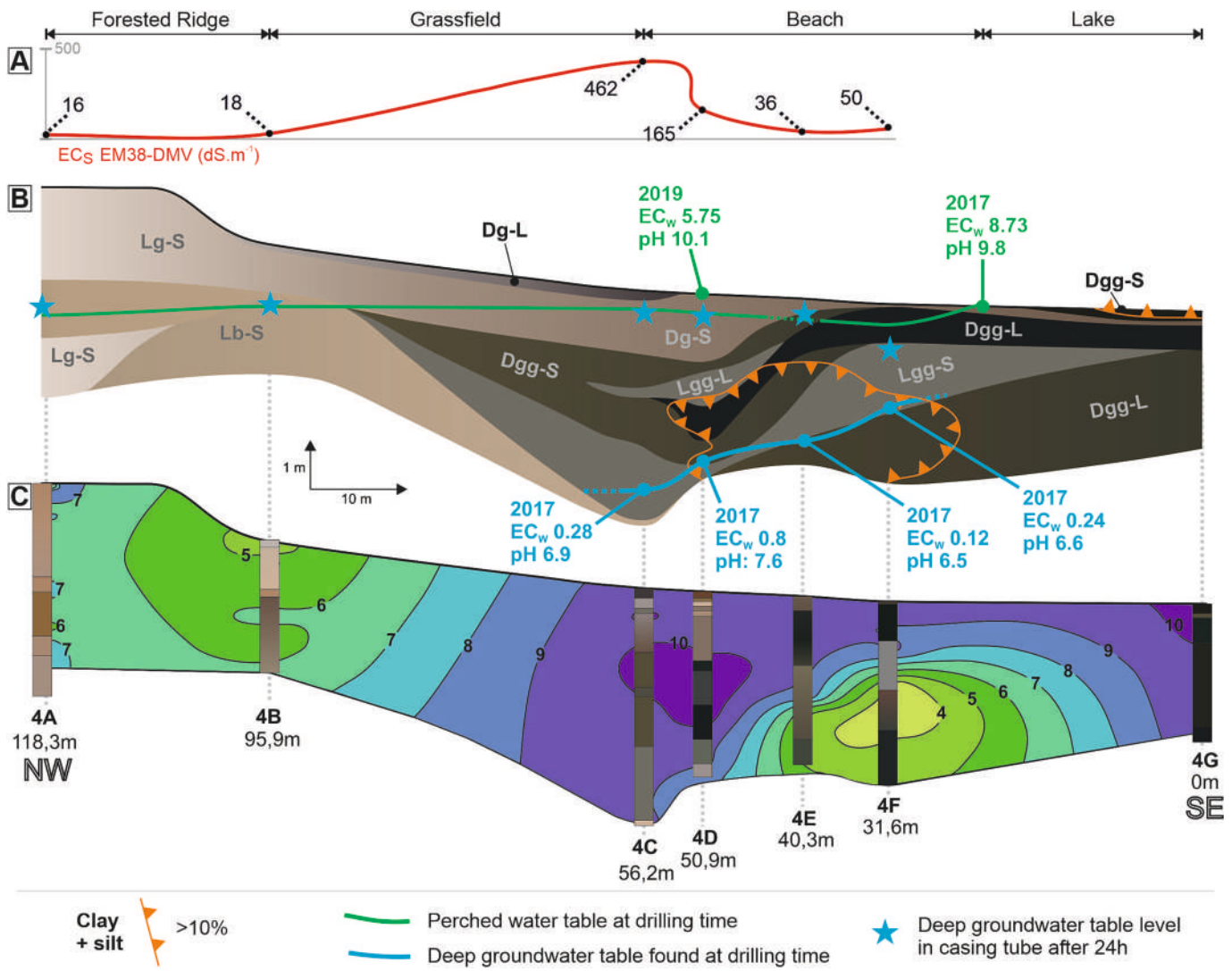

Fig. 10. T4 - Main characteristics of the 4-Green lake toposequence. (a) EMC_S profile; (b) soil horizons, water levels, fine fraction and EC_W values; c) soil pH. (For colour the reader is referred to the web version of this article).

marks the first precipitation stage in iron oxidation during hydrolysis, which may transform via the hematite or goethite transformation pathways depending on pH and moisture. Such transformations occur simultaneously, either by the condensation of ions or crystal dissolution in acidic (pH 3 to 4) and alkaline (pH > 8) conditions forming goethite, or by dehydration and internal atomic rearrangement of solid ferrihydrite in a neutral pH favoring hematite formation (Schwertmann et al., 1999; Cudennec and Lecerf, 2006). In the studied toposequences, such dynamics were not detected between hyperacid (pH < 4) and alkaline zones. More detailed studies of iron oxides would therefore be necessary to confirm or refute the hypotheses proposed by Merdy et al. (2022) relating to the formation of hyperacid horizons.

3.5. Chemical results

The average of all samples demonstrates the following succession: silica (SiO_2 = 91.84%), aluminum (Al_2O_3 = 2.22%), iron (Fe_2O_3 = 1.75%), potassium (K_2O = 0.75%), calcium (CaO = 0.30%), magnesium (MgO = 0.21%), titanium (TiO_2 = 0.18%), sodium (Na_2O = 0.11%), manganese (MnO = 0.11%) and phosphorus (P_2O_5 = 0.01%). The great dominance of SiO_2 is due to the high content of quartz sand in all samples. Relationships between the elements and the soil material texture and pH can be discussed from the PCA results (Fig. 14).

The first factorial axis is mainly defined by SiO_2 and sand on one side, and clay, silt and other elements on the other side. This is consistent with the differentiation between very sandy horizons and horizons with the presence of clay, often associated with other minerals (calcite, iron oxides). The second factorial axis is mainly defined by depth, Al_2O_3 and TiO_2 on one side, opposed to pH, CaO, MnO and Na_2O on the other side. The negative correlation between pH and depth is driven by high pH surface horizons near the lake and hyperacidic horizons at depth in the T1 and T4 sequences. The axis probably also differentiates acidic horizons richer in aluminous 1:1 clays (kaolinite) as indicated by the Al_2O_3 point, alkaline horizons richer in less aluminous 2:1 clays with K, Fe or Mg (Fe-illite, stevensite) as indicated by the K_2O, Fe_2O_3 and MgO points and evaporitic horizons as indicated by the Na_2O and the CaO points.

A correlation matrix was calculated assigning the lake characteristics (pH, EC, NTU, Redox) to all samples from the corresponding toposequence. The results revealed that there were no significant or interpretable correlations between the lake characteristics and soil parameters.

3.6. Possible active processes

The variations in granulometry, mineralogy and chemical composition of the soils observed along each toposequence result from

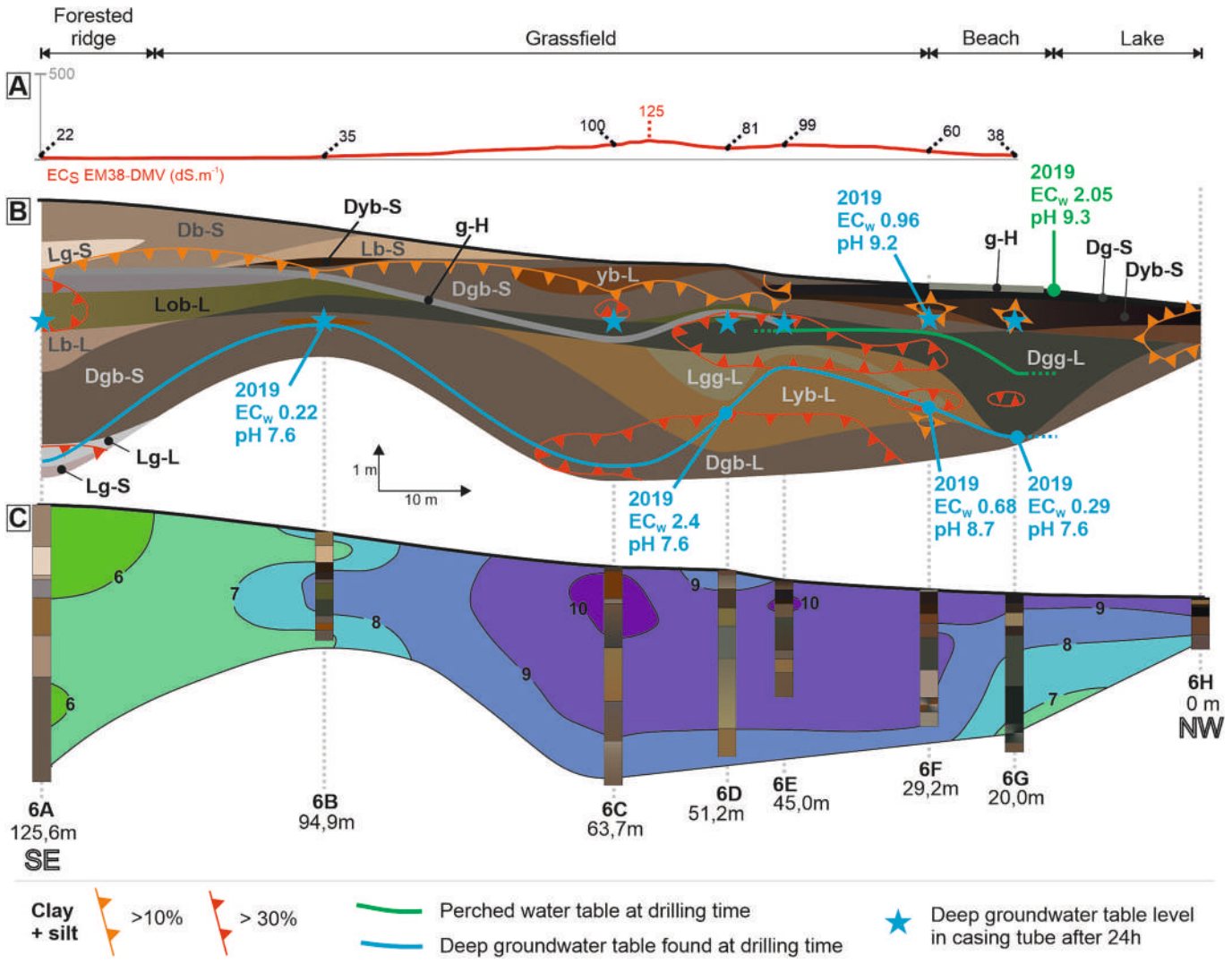

Fig. 11. T6 - Main characteristics of the 6-Black lake toposequence. (a) EMC_S profile; (b) soil horizons, water levels, fine fraction and EC_W values; c) soil pH. (For colour the reader is referred to the web version of this article).

neoformation, precipitation, dissolution, transformation, dehydration and mineral heritage acting on the site (Macías and Camps-Arbestain, 2020; Vidoca, 2020), all dependent on physicochemical properties of the soil solutions.

3.6.1. *Pedogenesis, hydrodynamics and lake type*

The observed soil mineralogy reflects the particularities of the Nhecolândia environment. Firstly, due to the nature of the parent sediment, there is a predominance of sandy materials, therefore very siliceous, with low levels of aluminum and good permeability. Secondly, the contrasting climate leads to two distinct environmental conditions during the rainy and dry seasons. During the rainy season, leaching occurs, with solutes supplied to lakes, whereas the dry season results in a confined environment where solutes concentrate in lakes and downslope soils. Thirdly, fluctuations in water levels throughout the climate cycle are decisive. In the case of freshwater lakes (*baías*), high water levels during the rainy season facilitates the flushing of solutes accumulated during the dry season into the main watercourses. Two non-exclusive processes can account for this flushing: lake overflow or deep leaching through groundwater (Sakamoto et al., 2004), with the latter supported by the observation that some freshwater lakes are separated from the floodplains by forested ridges (§3.2). Saline-alkaline lakes can form when low-permeability horizons create hydraulic disconnection between deep groundwater on one side and lakes and downslope perched water-tables on the other. Our investigation has confirmed the presence of such horizons, greenish and more clayey, in each of the studied toposequences (Figs. 9 to 12). We observed consistency between (1) the distribution of these greenish, more clayey horizons and (2) the hydraulic disconnection between alkaline, perched groundwater and acidic, deep groundwater. Contrary to the hypothesis proposed by Costa et al. (2015), we did not observe an overflow of non-alkaline groundwater sustaining the saline-alkaline lake during the dry season. On slopes, the greenish horizons formed a step which promotes endorheism in T1, T4 and T6. Such a step is less pronounced in T7, suggesting that the hydraulic isolation of the T7 crystalline lake has been less effective than for the other lakes. This could explain a lower confinement resulting in lower alkalinity, as evidenced by lower ECw and pH levels in the lake waters. These conditions do not reach the thresholds required to trigger algal blooms, as seen in the green lakes, nor do they reach the threshold for massive solubilization of organic matter, as observed in the black lakes. This study, however, did not identify factors that could explain the differentiation between black and green lakes.

3.6.2. *Hydrodynamics and mineral genesis*

The mineral composition observed at the sequence scale (§3.4) is closely related to hydrodynamics that impacts the chemistry of the

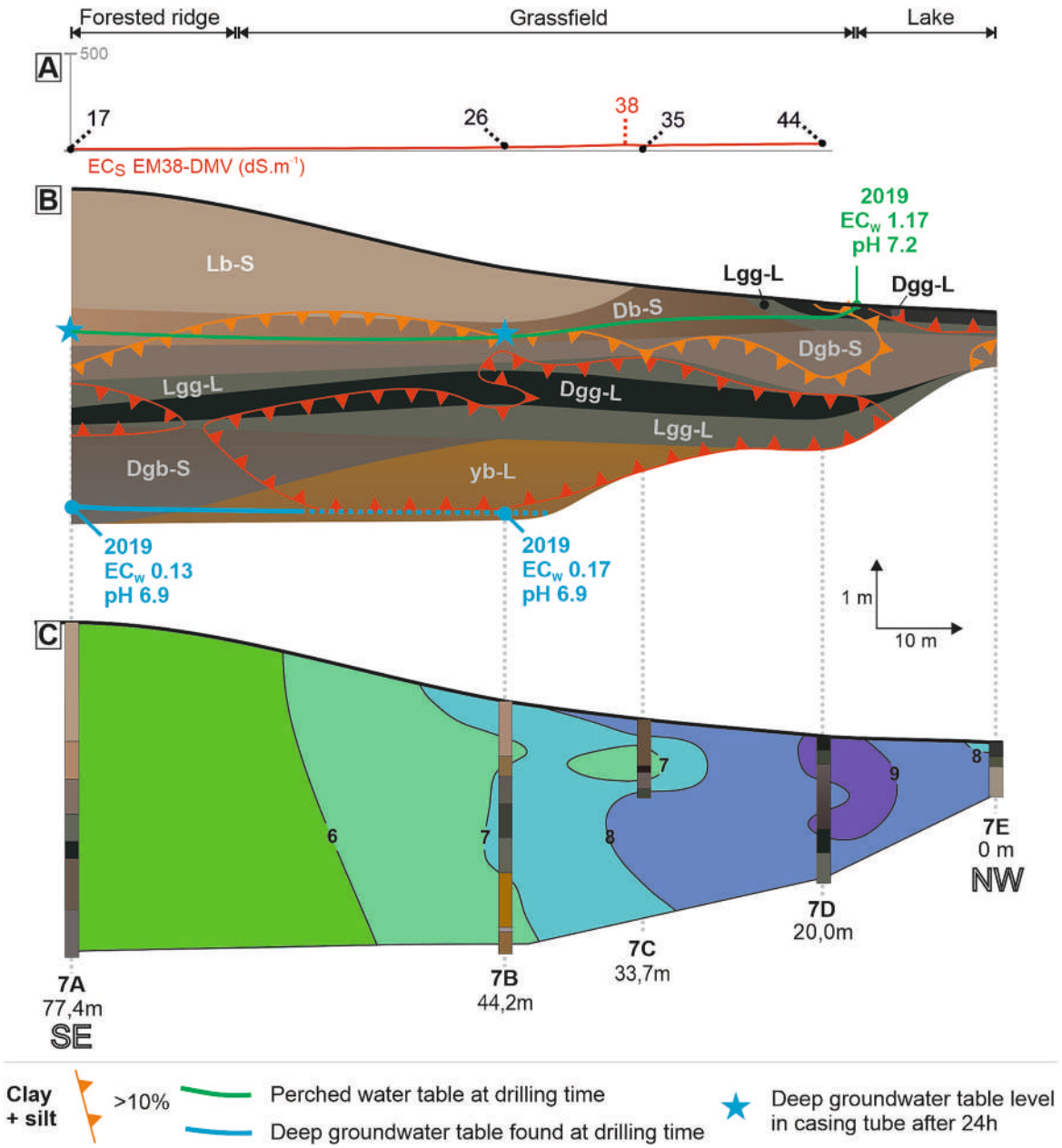

Fig. 12. T7 - Main characteristics of the 7-Crystalline lake toposequence. (a) EMC_S profile; (b) soil horizons, water levels, fine fraction and EC_W values; c) soil pH. (For colour the reader is referred to the web version of this article).

groundwater. The minerals identified here include feldspar, 1:1 clays, non-expandable 2:1 phyllosilicate, expandable 2:1 clays, secondary silica, iron oxides, and calcite. These findings align with previous research conducted in similar systems (Barbiero et al., 2008, 2016; Furquim et al., 2008, 2010a, 2010b). On the ridges, leached sandy horizons overlie horizons where primary minerals undergo dissolution and 1:1 (Fe-kaolinite) and 2:1 (Fe-illite, Fe-beidellite) minerals are formed. The downslope greenish horizons resulted from neoformations characteristic of confined environments (stevensite like clays, calcite).

Our data provide new insights into the precipitation conditions of secondary silica. Silcrete material can develop by secondary silica accumulation when there is an insufficient amount of Al compared to Si for phyllosilicate precipitation (Taylor and Eggleton, 2017). Here two types of silcrete were observed.

The first one formed below the leached sandy horizons, on the ridge and in the upper sections of slope (g-H horizon in T1 and T6). Silica precipitated in acidic (pH < 7), sandy material, from soil water concentrated through evaporation in the capillary fringe. The high Si/Al ratio was likely due to the percolating rainwater encountering only sandy materials.

The second one formed downslope on the topsoil (g-H horizon in T6). Silica precipitated in alkaline (pH > 9) material, from lake water transported within the soil by capillarity and concentrated at the soil surface through evaporation. In this setting, the high Si/Al ratio was favored by the high pH of the lake water that increased the quartz solubility and the quartz dissolution rate. Quartz dissolution rates were found to increase by 10 times at pH 9.5 compared to pH 7 (House and Orr, 1992) and even >20 times at the ionic strength of lake water compared to rainwater (Icenhower and Dove, 2000). As a result, black lake waters exhibit an average concentration of dissolved Si and Al at approximately 1.1 10^{-1} and 1.5 10^{-4} ml L^{-1}, respectively (Merdy et al., 2022). Hence, two distinct types of silcrete formations were identified within these systems: one occurring under neutral/acidic conditions and the other under alkaline conditions, both forming in an evaporating

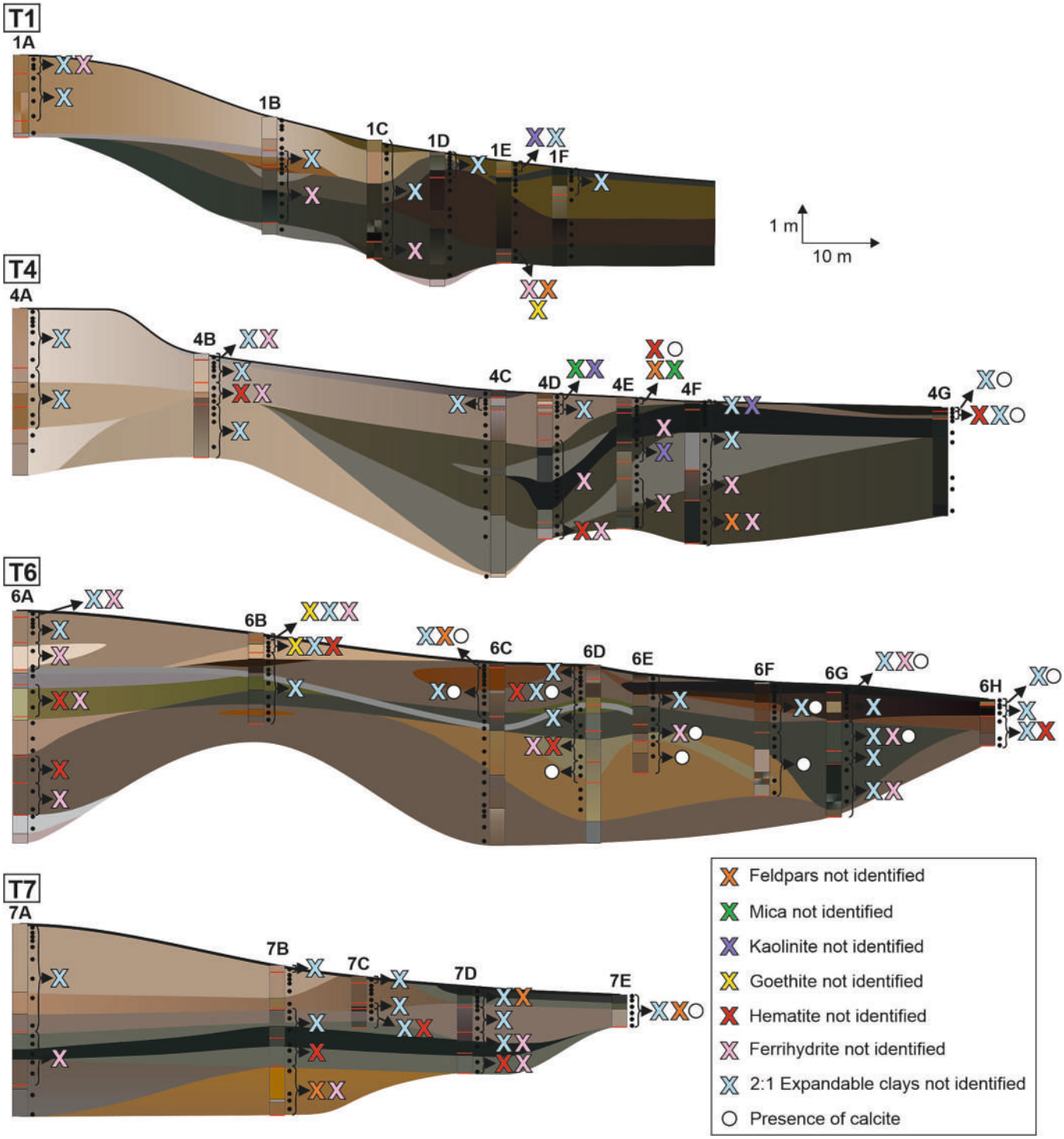

Fig. 13. Soil mineralogy - Main minerals along the sequences. Black points indicate the analyzed samples. Unless otherwise stated, the following minerals have been identified at each point: quartz, feldspars, micas, kaolinite, 2:1 expandable clay minerals, goethite, hematite, ferrihydrite. The figure therefore represents the absence of one or more of these minerals or the presence of calcite. (For colour the reader is referred to the web version of this article).

capillary fringe.

4. Conclusions

This research marks the initial stage of the studies of factors that determine the dynamics between different types of saline-alkaline lakes and nearby surrounding soils. The objective of verifying, on a single site, a set of results previously acquired by independent studies on many distinct Nhecolândia sites has been partially achieved. Our results confirmed the general organization of the soil cover around saline-alkaline lakes. The very sandy light brown soils of the ridges, which eventually present a silcrete type horizon at depth, give way down the slopes to greenish soils with, at depth, more clayey horizons with low permeability. These establish a hydraulic discontinuity between the slightly acidic groundwater of the general, deep groundwater and the very alkaline perched groundwater. Our 45-month time sequence of satellite data confirmed that the studied saline-alkaline lakes remained isolated from the ephemeral superficial flood channels. Some freshwater

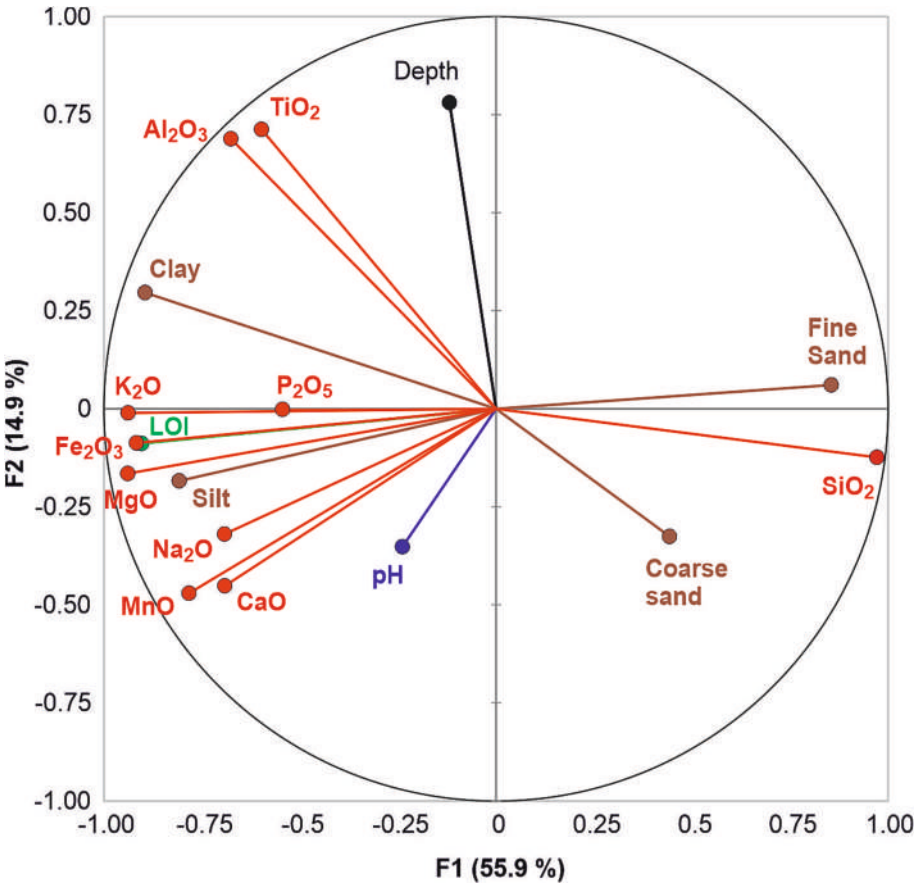

Fig. 14. Statistical data - PCA correlation circle between variables. Percentage on each factorial axis gives the explained variance. LOI: loss on ignition.

lakes, however, also remained isolated, which shows that the leaching of labile elements out of the lake catchment can occur via other processes than surface flushing, such as deep drainage or groundwater flushing. This shows that hydraulic discontinuity between surface groundwater on lake slopes and deep groundwater is a necessary condition for the acquisition of the saline-alkaline character of the lakes. Our results also suggested that some saline-alkaline lakes may remain crystalline due to slightly lower alkalinity as a result of less efficient hydraulic discontinuity between deep groundwater and alkaline lake and soil water. The alkalinity of crystalline lakes would remain too low to allow a cyanobacteria bloom or the maintenance of organic matter in solution.

The present study confirmed the presence and location on the slopes of hyperacidic horizons, located downslope beneath the more alkaline horizons and attributed to the mixing of alkaline and acidic water. The validation of such a mechanism will however require more detailed mineralogical investigations. It also remains to verify the mineralogy of 2:1 minerals associated with deep ridge soil horizons and slope alkaline horizons.

Declaration of Competing Interest

The authors declare that they have no known competing financial interests or personal relationships that could have appeared to influence the work reported in this paper.

Data availability

Raw data is given as supplementary material.

Acknowledgements

This work was supported by the São Paulo Research Foundation (FAPESP) [grant numbers #2016/14227-5 and #2019/21157-1] and the Brazilian National Council for Scientific and Technological Development (CNPq) [grant number CRM #307024/2018-0].

Appendix A. Supplementary data

Supplementary data to this article can be found online at https://doi.org/10.1016/j.geodrs.2023.e00746.

References

Acevedo, N.I.A., Rocha, M.C.G., Bertolino, L.C., 2017. Mineralogical characterization of natural clays from Brazilian southeast region for industrial applications. Cerâmica 63, 253–262. https://doi.org/10.1590/0366-69132017633662045.

Alho, C.J.R., 2008. Biodiversity of the Pantanal: response to seasonal flooding regime and to environmental degradation. Braz. J. Biol. 68 (4 suppl), 957–966. https://doi.org/10.1590/S1519-69842008000500005.

Almeida, T.I.R.A., Fernandes, E., Mendes, D., Branco, F.C., Sígolo, J.B., 2007. Distribuição espacial de diferentes classes de Lagoas no Pantanal da Nhecolândia, MS, a partir de dados vetoriais e SRTM: uma contribuição ao estudo de sua compartimentação e gênese. Geol. USP 7 (2). https://doi.org/10.5327/Z1519-874x2007000200007.

Alves, S.M.F., Alcântara, G.R., Reis, E.F., Queiroz, D.M., Valente, D.S.M., 2013. Definição de zonas de manejo a partir de mapas de condutividade elétrica e matéria orgânica. Biosci. J. Uberlândia 29, 104–114. Available from: https://seer.ufu.br/index.php/biosciencejournal/article/view/13687.

Anderson, J.U., 1963. An improved pretreatment for mineralogical analysis of samples containing organic matter. Clay Clay Miner. 10, 380–388. https://doi.org/10.1346/CCMN.1961.0100134.

Andrade, G.R.P., Furquim, S.A.C., Nascimento, T.T.V., Brito, A.C., Camargo, G.R., Souza, G.C., 2020. Transformation of clay minerals in salt-affected soils, Pantanal wetland, Brazil. Geoderma 371, 114380. https://doi.org/10.1016/j.geoderma.2020.114380.

Assine, M.L., Merino, E.R., Pupim, F.N., Warren, L.V., Guerreiro, R.L., McGlue, M.M., 2015. Geology and geomorphology of the Pantanal Basin. In: Bergier, I., Assine, M.L. (Eds.), Dynamics of the Pantanal Wetland in South America, pp. 23–50. https://doi.org/10.1007/698_2015_349.

Barbiero, L., Queiroz-Neto, J.P., Ciornei, G., Sakamoto, A.Y., Capellari, B., Fernandes, E., Vallès, V., 2002. Geochemistry of water and ground water in the Nhecolândia, Pantanal of Mato Grosso, Brazil: variability and associated processes. Wetlands 22 (3), 528–540. https://doi.org/10.1672/0277-5212(2002)022[0528,GOWAGW]2.0.CO;2.

Barbiero, L., Rezende-Filho, A.T., Furquim, S.A.C., Furian, S., Sakamoto, A.Y., Vallès, V., Graham, R.C., Fort, M., Ferreira, R.P.D., Queiroz-Neto, J.P., 2008. Soil morphological control of hydrogeochemistry in a saline and freshwater lake landscape in the Pantanal of Nhecolândia, Brazil. Geoderma 148, 91–106. https://doi.org/10.1016/j.geoderma.2008.09.010.

Barbiero, L., Berger, G., Rezende Filho, A.T., Meunier, J.-F., Martins-Silva, E.R., Furian, S., 2016. Organic control of dioctahedral and trioctahedral clay formation in an alkaline soil system in the Pantanal wetland of Nhecolândia, Brazil. PLoS One 11 (7), e0159972. https://doi.org/10.1371/journal.pone.0159972. Jul 27.

Boulet, R., Humbel, F.-X., Lucas, Y., 1982. Analyse structurale et cartographie en pédologie. I- Prise en compte de l'organisation bidimensionnelle de la couverture pédologique: les études de toposéquences et leurs principaux apports à la connaissance des sols. Cah ORSTOM, sér Pédol XIX, 309–321. Available from: https://www.documentation.ird.fr/hor/fdi:03252.

Cornell, R.M., Schwertmann, U., 2000. Iron Oxides in the Laboratory: Preparation and Characterization, 2nd edition. WILEY-VCH, Weinheim.

Costa, M.P.F., Telmer, K.H., Evans, T.L., Almeida, T.I.R., Diakun, M.T., 2015. The lakes of the Pantanal: inventory, distribution, geochemistry, and surrounding landscape. Wetl. Ecol. Manag. 23, 19–39. https://doi.org/10.1007/s11273-014-9401-3.

Cotta, S.R., Pellegrinetti, T.A., Andreote, A.P.D., Costa, J.S., Sarmento, H., Fiore, M.F., 2022. Disentangling the lifestyle of bacterial communities in tropical soda lakes. Sci. Rep. 12 https://doi.org/10.1038/s41598-022-12046-2 art. 7939.

Cudennec, Y.C., Lecerf, A., 2006. The transformation of ferrihydrite into goethite or hematite, revisited. J. Solid State Chem. 179 (2006), 716–722. https://doi.org/10.1016/j.jssc.2005.11.030.

Cunha, N.G., 1980. Considerações sobre os solos da sub-região da Nhecolândia, Pantanal Mato-Grossense. Corumbá, EMBRAPA-EUPAE de Corumbá. Circular técnico 1. Available from: https://www.infoteca.cnptia.embrapa.br/handle/doc/787697.

Curti-Martins, E.R., 2012. Tipologia de Lagoas Salinas no Pantanal da Nhecolândia (MS). Thesis. Universidade de São Paulo, São Paulo. Available from: https://www.teses.usp.br/teses/disponiveis/8/8135/tde-14012013-172446/pt-br.php.

Ekosse, G.I.E., 2005. Fourier transform infrared spectrophotometry and X-ray powder diffractometry as complementary techniques in characterizing clay size fraction of kaolin. J. Appl. Sci. Environ. Manag. 9 (2), 43–48. https://doi.org/10.4314/jasem.v9i2.17289.

EMBRAPA, 2017. Manual de Métodos de Análise de Solo. (3ed ampl). Brasília. Available from: https://www.embrapa.br/busca-de-publicacoes/-/publicacao/1085209/manual-de-metodos-de-analise-de-solo.

Freitas, J.G., Furquim, S.A.C., Aravena, R., Cardoso, E.L., 2019. Interaction between lakes' surface water and groundwater in the Pantanal wetland, Brazil. Environ. Earth Sci. 78, 139. https://doi.org/10.1007/s12665-019-8140-4.

Furian, S., Curti-Martins, E.R., Parizotto, T.M., Rezende-Filho, A.T., Victoria, R.L., Barbiero, L., 2013. Chemical diversity and spatial variability in myriad lakes in Nhecolândia in the Pantanal wetlands of Brazil. Limnol. Oceanogr. 58, 2249–2261. Available from: https://hal.archives-ouvertes.fr/hal-02043233.

Furquim, S.A.C., Graham, R.C., Barbiero, L., Queiroz-Neto, J.P., Vallès, V., 2008. Mineralogy and genesis of smectites in an alkaline-saline environment of Pantanal wetland, Brazil. Clay Clay Miner. 56, 579–595. https://doi.org/10.1346/CCMN.2008.0560511.

Furquim, S.A.C., Graham, R.C., Barbiero, L., Queiroz-Neto, J.P., Vidal-Torrado, P., 2010a. Soil mineral genesis and distribution in a saline lake landscape of the Pantanal wetland, Brazil. Geoderma 154, 518–528. https://doi.org/10.1016/j.geoderma.2009.03.014.

Furquim, S.A.C., Barbiero, L., Graham, R.C., Queiroz-Neto, J.P., Ferreira, R.P.D., Furian, S., 2010b. Neoformation of micas in soils surrounding an alkaline-saline lake of Pantanal wetland, Brazil. Geoderma 158, 331–342. https://doi.org/10.1016/j.geoderma.2010.05.015.

Google, 2020. Google Earth Engine API. Avaiable from. https://developers.google.com/earth-engine. Acessed at June 2nd, 2020.

Guerreiro, R.L., 2016. Mudanças paleoambientais no holoceno em lagoas salinas do Pantanal da Nhecolândia. Thesis. Universidade Estadual Paulista, Rio Claro. Available from: https://repositorio.unesp.br/handle/11449/147123.

Guerreiro, R.L., Bergier, I., McGlue, M.M., Warren, L.V., Abreu, U.G.P., Abrahão, J., Assine, M.L., 2019. The soda lakes of Nhecolandia: a conservation opportunity for the Pantanal wetlands. Perspect. Ecol. Conserv. 17 (1), 9–18. https://doi.org/10.1016/j.pecon.2018.11.002.

Hamilton, S.K., Souza, O.C., Coutinho, M.E., 1998. Dynamics of floodplain inundation in the alluvial fan of the Taquari River (Pantanal, Brazil). SIL Proc. 1922–2010 (26), 916–922. https://doi.org/10.1080/03680770.1995.11900852.

House, W.A., Orr, D.R., 1992. Investigation of the pH dependence of the kinetics of quartz dissolution at 25 C. J. Chem. Soc. Faraday Trans. 88 (2), 233–241. https://doi.org/10.1039/FT9928800233.

Icenhower, J.P., Dove, P.M., 2000. The dissolution kinetics of amorphous silica into sodium chloride solutions: effects of temperature and ionic strength. Geochim. Cosmochim. Acta 64 (24), 4193–4203. https://doi.org/10.1016/S0016-7037(00)00487-7.

Instituto Nacional de Meteorologia - INMET, 2020. Banco de Dados Meteorológicos para Ensino e Pesquisa - BDMEP. Brasília, DF, Brasil. Disponível em: http://www.inmet.gov.br/portal/index.php?r=bdmep/bdmep (accessed at 9 march 2020).

Ishida, D.A., Montes, C.R., Lucas, Y., Pereira, O.J.R., Merdy, P., Melfi, A.J., 2014. Genetic relationships between ferralsols, podzols and white kaolin in Amazonia. Eur. J. Soil Sci. 65, 706–717. https://doi.org/10.1111/ejss.12167.

Jackson, M.L., 1985. Soil Chemical Analysis Advanced Course, 5th Print. Department of Soil Science University, Wisconsin, Madison WI, p. 894.

Ji, J., Ge, Y., Balsam, W., Damuth, J.E., Chen, J., 2009. Rapid identification of dolomite using a Fourier transform infrared spectrophotometer (FTIR): a fast method for identifying Heinrich events in IODP site U1308. Mar. Geol. 258, 60–68. https://doi.org/10.1016/j.margeo.2008.11.007.

Jolliffe, I.T., 2002. Principal Component Analysis, 2nd ed. Springer-Verlag, New York.

Kosmas, C.S., Curi, N., Bryant, R.B., Franzmeier, D.P., 1984. Characterization of iron oxide minerals by second derivative visible spectroscopy. Soil Sci. Soc. Am. J. 48 (2), 401–405. https://doi.org/10.2136/sssaj1984.03615995004800020036x.

Lainé, M., Balan, E., Allard, T., Paineau, E., Jeunesse, P., Mostafavi, M., Robert, J.-L., Le Caër, S., 2017. Reaction mechanisms in swelling clays under ionizing radiation: influence of the water amount and of the nature of the clay mineral. RSC Adv. 7 (256), 526–534. https://doi.org/10.1039/C6RA24861F.

Li, X., Chang, S.X., Salifu, K.F., 2014. Soil texture and layering effects on water and salt dynamics in the presence of a water table: a review. Environ. Rev. 22 (1), 41–50. https://doi.org/10.1139/er-2013-0035.

Macías, F., Camps-Arbestain, M., 2020. A biogeochemical view of the world reference base soil classification system: homage to Ward Chesworth. Adv. Agron. 160 https://doi.org/10.1016/bs.agron.2019.11.002.

Malengrau, N., Bedidi, A., Muller, J.-P., Herbillon, A.J., 1996. Spectroscopic control of iron oxide dissolution in two ferralitic soils. Eur. J. Soil Sci. 47, 13–20. https://doi.org/10.1111/j.1365-2389.1996.tb01367.x.

Mariot, M., Dudak, Y., Furian, S., Sakamoto, A., Vallès, V., Fort, M., Barbiero, L., 2007. Dissolved organic matter fluorescence as a water flow tracer in the tropical wetland of Pantanal of Nhecolândia, Brazil. Sci. Total Environ. 388, 183–196. https://doi.org/10.1016/j.scitotenv.2007.08.003.

Merdy, P., Gamrani, M., Montes, C.R., Rezende-Filho, A.T., Barbiero, L., Ishida, D.A., Silva, A.R.C., Melfi, A.J., Lucas, Y., 2022. Processes and rates of formation defined by modelling in alkaline to acidic soil systems in Brazilian Pantanal wetland. Catena 210, 105876. https://doi.org/10.1016/j.catena.2021.105876.

Munsell Color (Firm), 1954. Munsell Soil Color Charts. Baltimore.

Nash, D.J., Ullyott, J.S., 2007. Silcrete. In: Nash, D.J., McLaren, S.J. (Eds.), Geochemical Sediments and Landscapes. Blackwell Publishing, Oxford, UK, pp. 95–148. https://doi.org/10.1002/9780470712917.

Oliveira Júnior, J.C., Andrade, G.R.P., Barbiero, L., Furquim, S.A.C., Vidal-Torrado, P., 2020. Flooding effect on mineralogical and geochemical changes in alkaline-sodic soil system of northern Pantanal wetlands. Brazil. Eur. J. Soil Sci. 71 (3), 433–447. https://doi.org/10.1111/ejss.12871.

Pansu, M., Gautheyrou, J., 2006. Particle size analysis. In: Handbook of Soil Analysis. Springer, Berlin, Heidelberg, pp. 15–63. https://doi.org/10.1007/978-3-540-31211-6_2.

Pellegrinetti, T.A., Cotta, S.R., Sarmento, H., Costa, J.S., Delbaje, E., Montes, C.R., Camargo, P.B., Barbiero, L., Rezende-Filho, A.T., Fiore, M.F., 2022. Bacterial communities along environmental gradients in tropical soda lakes. Microb. Ecol. https://doi.org/10.1007/s00248-022-02086-6.

Pereira, O.J.R., Merino, E.R., Montes, C.R., Barbiero, L., Rezende-Filho, A.T., Lucas, Y., Melfi, A.J., 2020. Estimating water pH using cloud-based landsat images for a new classification of the Nhecolândia Lakes (Brazilian Pantanal). Remote Sens. 12, 1090. https://doi.org/10.3390/rs12071090.

Planet Labs, 2016. Planet Imagery Product Specification, 56. Planet Labs, São Francisco.

Ramos, M.D., Merino, E.R., Montes, C.R., Melfi, A.J., 2023. Avaliação do Uso Integrado de Imagens de Nanossatélites e Classificadores baseados em Aprendizado de Máquina para Estudos da Dinâmica Hidrológica na Região da Nhecolândia (Pantanal). Rev. Bras. Cartogr. 75, 1. https://doi.org/10.14393/revbrascartogr.

Russell, J.D., Fraser, A.R., 1994. Infrared methods. In: Wilson, M.J. (Ed.), Clay Mineralogy: Spectroscopic and Chemical Determinative Methods. Chapman and Hall, London, pp. 11–67. https://doi.org/10.1007/978-94-011-0727-3_2.

Saikia, B.J., Parthasarathy, G., Sarmah, N.C., 2008. Fourier transform infrared spectroscopic estimation of crystallinity in SiO2 based rocks. Bull. Mater. Sci. 31 (5), 775–779. https://doi.org/10.1007/s12034-008-0123-0.

Sakamoto, A.Y., Sakamoto, L.L.S., Neto, J.P.Q., Barbiero, L., 2004. Abordagem metodológica para o estudo de lagoas e Salinas do Pantanal da Nhecolândia, MS: fazenda São Miguel do Firme. In: IV Simp. Sobre Rec. Nat. e sócio-econômicos do Pantanal. Corumbá. Available from: https://docplayer.com.br/87510495-Abordagem-metodologica-para-o-estudo-de-lagoas-e-salinas-do-pantanal-da-nhecolandia-ms-fazenda-sao-miguel-do-firme.html.

Salis, S.M., Lehn, C.R., Mattos, P.P., Bergier, I., Crispim, S.M.A., 2014. Root behavior of savanna species in Brazil's Pantanal wetland. Glob. Ecol. Conserv. 2, 378–384. https://doi.org/10.1016/j.gecco.2014.10.009.

Scheinost, A.C., Chavernas, A., Barrón, V., Torrent, T., 1998. Use and limitations of second-derivative diffuse reflectance spectroscopy in the visible to near-infrared range to identify and quantify Fe oxide minerals in soils. Clay Clay Miner. 46 (5), 528–536. https://doi.org/10.1346/CCMN.1998.0460506.

Schwertmann, U., Friedl, J., Stanjek, H., 1999. From Fe(III) ions to ferrihydrite and then to hematite. J. Colloid Interface Sci. 209, 215. https://doi.org/10.1006/jcis.1998.5899.

Souza Oliveira, N., Schiavo, J.A., Souza, A.C., Laranjeira, L.T., Moraes, E.M.V., Pereira, M.G., 2021. Mineralogy and genesis in an alkaline soil system in the

southern Pantanal wetland, Brazil. S. Am. Earth Sci. J. 111, 103456 https://doi.org/10.1016/j.jsames.2021.103456.
Taylor, G., Eggleton, R.A., 2017. Silcrete: an Australian perspective. Aust. J. Earth Sci. 64 (8), 987–1016. https://doi.org/10.1080/08120099.2017.1318167.
Theodosoglou, E., et al., 2010. Comparative fourier transform infrared and x-ray powder diffraction analysis of naturally occurred k-feldspars. Bull. Geol. Soc. Greece XLIII (5), 2752. https://doi.org/10.12681/bgsg.11681.
USDA. United States Department of Agriculture, 1987. Soil Mechanics Level 1, Module 3, USDA Soil Textural Classification Study Guide. USDA Soil Conservation Service, Washington DC.
Vaculíková, L., Plevová, E., 2005. Identification of clay minerals and micas in sedimentary rocks. Acta Geodyn. Geomater. 2 (2 (138)), 167–175. Available at: https://www.irsm.cas.cz/materialy/acta_content/2005_02/20_Vaculikova.pdf.
Vidoca, T.T., 2020. Gênese de argilominerais em solos afetados por sais no entorno de lagoas salobras do Pantanal da Nhecolândia. Dissertation. Universidade de São Paulo, São Paulo. https://doi.org/10.11606/D.8.2020.tde-23092020-171253.
Wilson, M.J., 1987. X-ray powder diffraction methods. In: Wilson, M.J. (Ed.), A Handbook of Determinative Methods in Clay Mineralogy. Chapman and Hall, New York, pp. 26–98.
Zhang, Y.G., Ji, J., Balsam, W.L., Liu, L., Chen, J., 2007. High Resolution Hematite and Goethite Records from ODP 1143, South China Sea: Co-Evolution of Monsoonal Precipitation and El Nino over the Past 600,000 Years. https://doi.org/10.1016/j.epsl.2007.09.022.
Zhou, J., Lau, K.-M., 1998. Does a monsoon climate exist over South America? J. Clim. 11, 1020–1040. https://doi.org/10.1175/1520-0442(1998)011<1020:DAMCEO>2.0.CO;2.
Zviagina, B.B., Drits, V.A., Dorzhieva, O.V., 2020. Distinguishing features and identification criteria for K-dioctahedral 1M micas (illite-aluminoceladonite and illite-glauconite-celadonite series) from middle-infrared spectroscopy data. Minerals 10, 153. https://doi.org/10.3390/min10020153.